Electronic Supplementary Material (ESI) for Physical Chemistry Chemical Physics.

Supplementary material: Trajectory-dependent threshold effects of proton stopping power in LiF nanosheet

Ya-Ting Sun,[1] Feng Wang,[1,*] and Cong-Zhang Gao[2,†]

[1]*Beijing Institute of Technology, Beijing 100081, China*

[2]*Institute of Applied Physics and Computational Mathematics, Beijing 100094, China*

(Dated: May 28, 2024)

In this Supplemental Material, we provide detailed computational information and additional results. The content is structured as follows:

A. Computational details of cut-off energy, k-points, supercell size, the state of the target atom, exchange-correlation approximations, vacuum layer;

B. Small displacement in the x- and y-directions when protons pass through the LiF nanosheet;

C. Kinetic energy loss of the proton as a function of displacement for channel-2 and channel-3;

D. Density of states distribution at proton velocities of 0.2 a.u. and 0.5 a.u.;

E. Differences in the average electron numbers of F and Li atoms at different energy levels with a proton velocity of 0.5 a.u.

*Electronic address: wangfeng01@tsinghua.org.cn

†Electronic address: czgao88@hotmail.com

A. Computational details

To investigate the impact of the basis set in the plane-wave expansion, we employed a significantly higher plane-wave kinetic cutoff energy of 130 Ry. It shown that the cutoff energy of 116 Ry exceeds the requirement for achieving convergence in ground-state properties (see Figure S1(a)). An additional factor contributing to the underestimation of the S_e at high velocities could be the undersampling of the Brillouin region due to the single Gamma-point approximation. To address this issue, a rt-TDDFT simulation was conducted for two proton velocities using only the single Gamma-point. It was observed that increasing the k-point sampling in the Brillouin region had low impact on the calculated the S_e. In order to improve the calculation accuracy, four k-points were used in the simulation (see Figure S1(b)). Finite size errors may be a potential factor contributing to the underestimation of the S_e at high velocities. Figure S1(c) illustrates the S_e obtained using a large 288-atom supercell containing 1440-electrons. It is evident from the figure that finite size errors are low and do not account for the underestimation observed in the S_e curve for the high-velocity range.

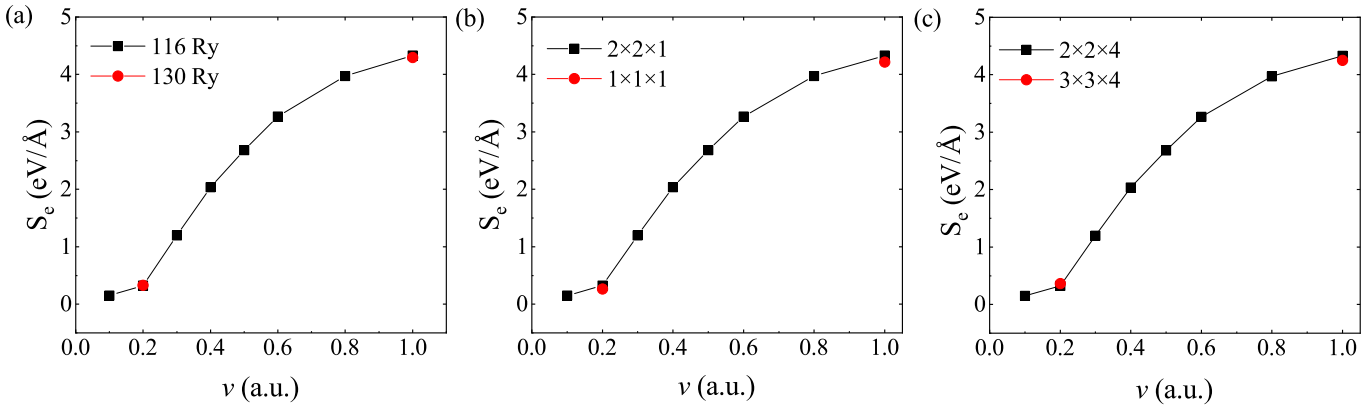

FIG. S1: The S_e as a function of the velocity of a proton in the LiF nanosheet is presented, demonstrating the convergence of the S_e curves with respect to various parameters: (a) Calculations performed with plane-wave kinetic cutoff energies of 116 Ry and 130 Ry. (b) Calculations carried out with four k-points in the Brillouin zone and only the Gamma-point in the Brillouin zone. (c) Calculations conducted using a 288-atom supercell and a 128-atom supercell. These tests were conducted under channel-1.

In our simulation, we explored the impact of fixed and unfixed target atoms on the S_e. Interestingly, we observed that fixing the target atoms had minimal effect on S_e, as illustrated in Figure S2(a). It is important to note that in our simulation process, we chose not to fix the target atoms. We conducted a comparison between two exchange-correlation (XC) approximations. Figure S2(b) illustrates the impact of two distinct approximation types, namely local density approximation (LDA) and the adiabatic generalized gradient

approximation (GGA), on the calculations, revealing a negligible difference between the two. Taking into account the trade-off between accuracy and computational efficiency, we opted for the GGA. To investigate the impact of the vacuum layer on the S_e, the results for three different models are presented in Figure S2(c). In all three models, the distance between the proton and the LiF nanosheet surface remains constant. The results indicate that the thickness of the vacuum layer has an impact on the S_e, and as the thickness of the vacuum layer increases, the S_e gradually increases and tends towards equilibrium.

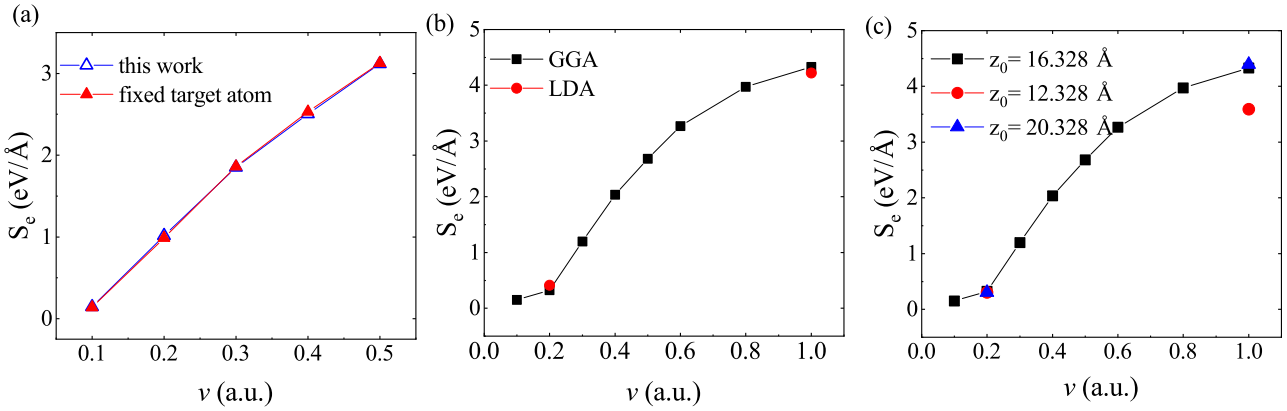

FIG. S2: (a) The S_e as a function of the velocity of a proton under channel-3 in the LiF nanosheet is presented using two models. This work does not involve fixed target atoms. (b) Shows the impact of two different XC approximation types, LDA and GGA, on the calculation. (c) The influence of the thickness of the vacuum layer on the S_e is shown. Figures (b) and (c) tests were conducted under channel-1.

B. Small displacements

TABLE S1: The values of "small displacements" observed in the x- and y-directions when protons pass through the LiF nanosheet at a velocity of 0.2 a.u.

trajectory	channel-1	channel-2	channel-3
small displacements (Å)	1.64471E-4	0.11488	0.28721

C. Kinetic energy loss of the proton for channel-2 and channel-3

In Figure S3, the kinetic energy loss of the proton as a function of the displacement for channel-2 and channel-3 are shown. It exhibit the same properties as channel-1.

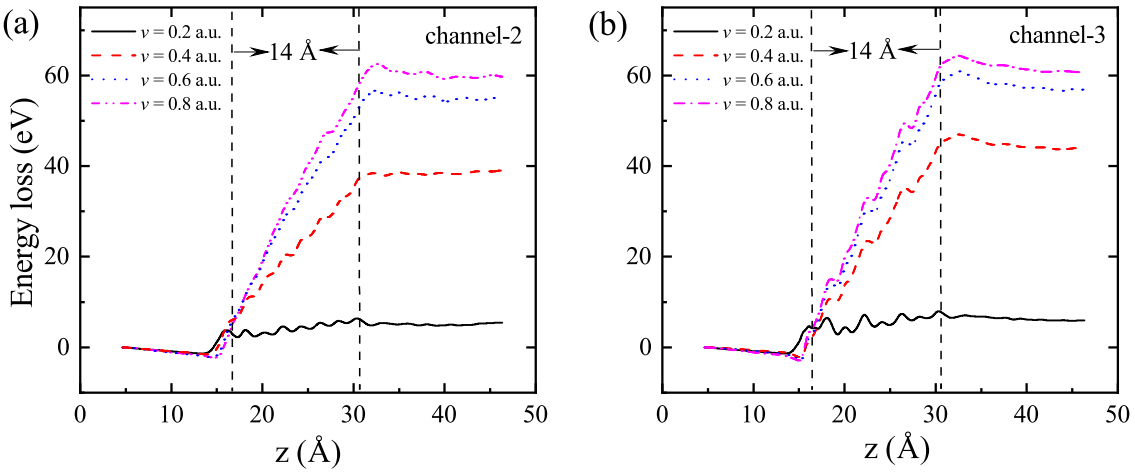

FIG. S3: The kinetic energy loss $\Delta E_{\mathrm{k,proton}} = E_{\mathrm{k,proton}}(0) - E_{\mathrm{k,proton}}(z)$ of protons as a function of the displacement for different velocities along (a) channel-2 and (b) channel-3.

D. Density of states

Figures S4 and S5 respectively show the DOS distribution along channel-2 and channel-3 when the proton velocity is 0.2 a.u. In addition, Figures S6-S8 show the results at the proton velocity of 0.5 a.u.

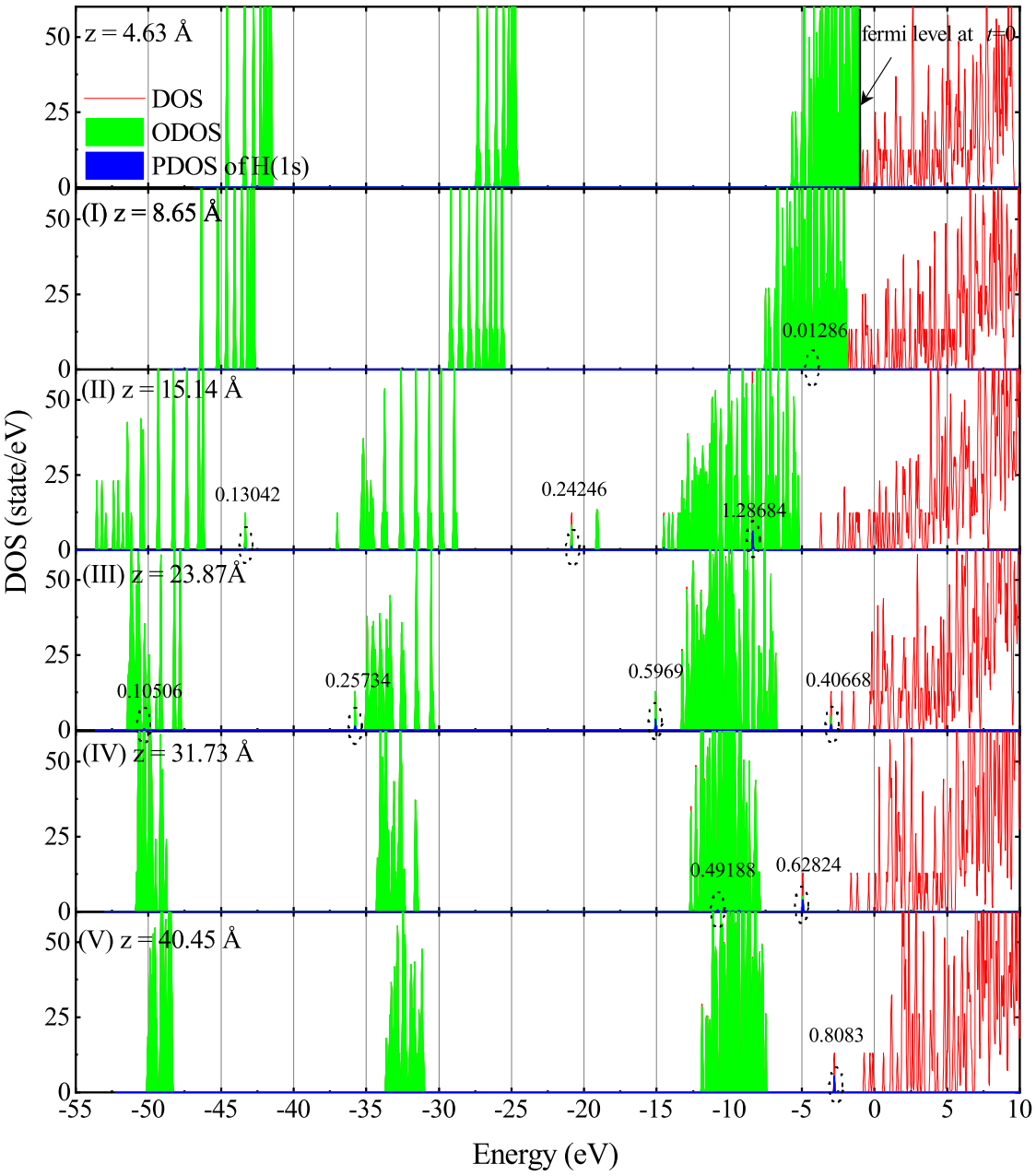

FIG. S4: Snapshots of DOS, ODOS, and PDOS show the projectiles with an incidence velocity of 0.2 a.u. located at z = 4.63, 8.65, 15.14, 23.87, 31.73, and 40.45 Å, respectively, under channel-2. The initial position of the Fermi level is indicated. The dashed ellipse represents the position of the adiabatic eigenstates that contribute to the H(1s) state, while the number of electrons occupying the H(1s) state within the elliptical area is shown above it.

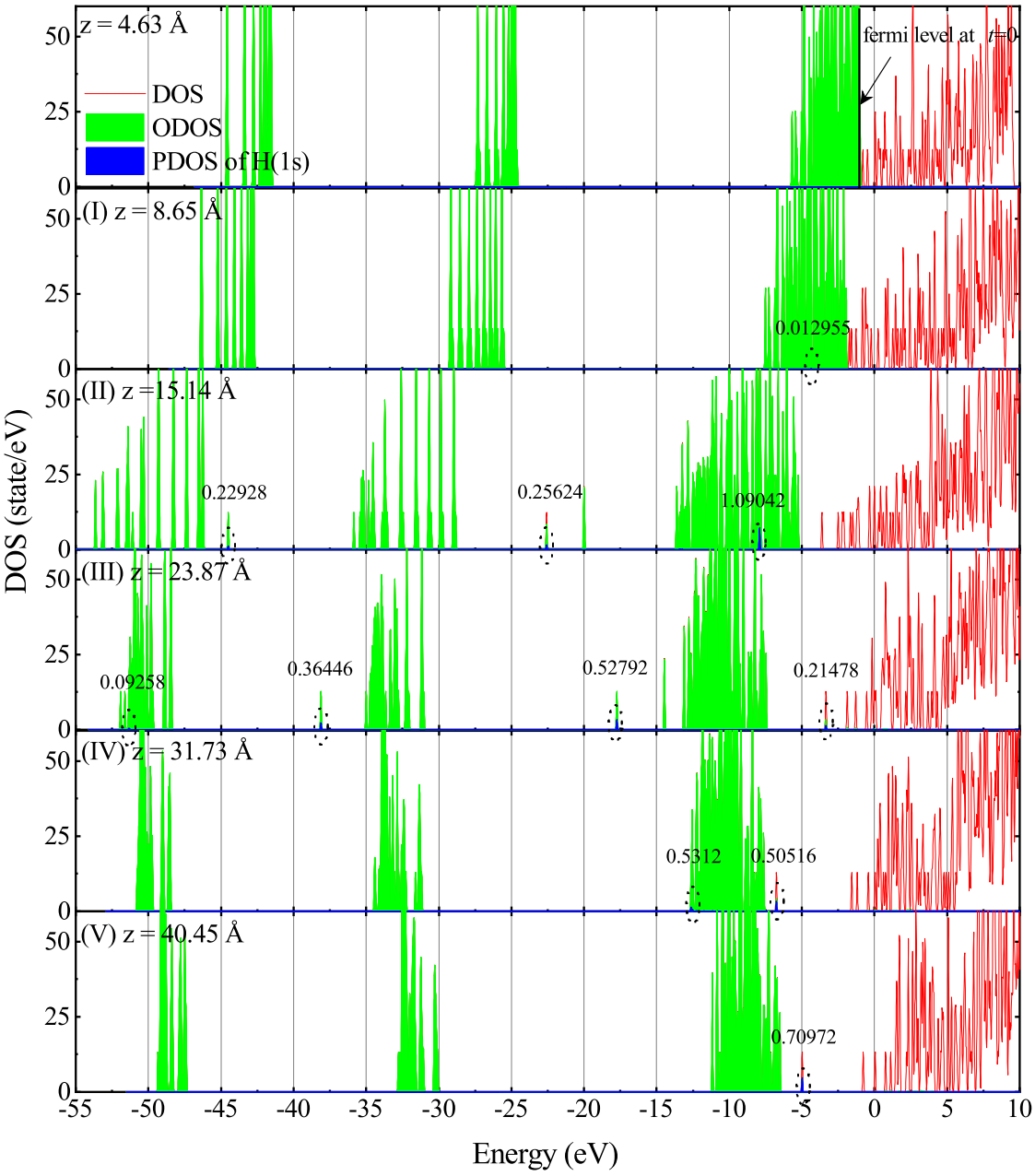

FIG. S5: Same as Figure S4, but under channel-3.

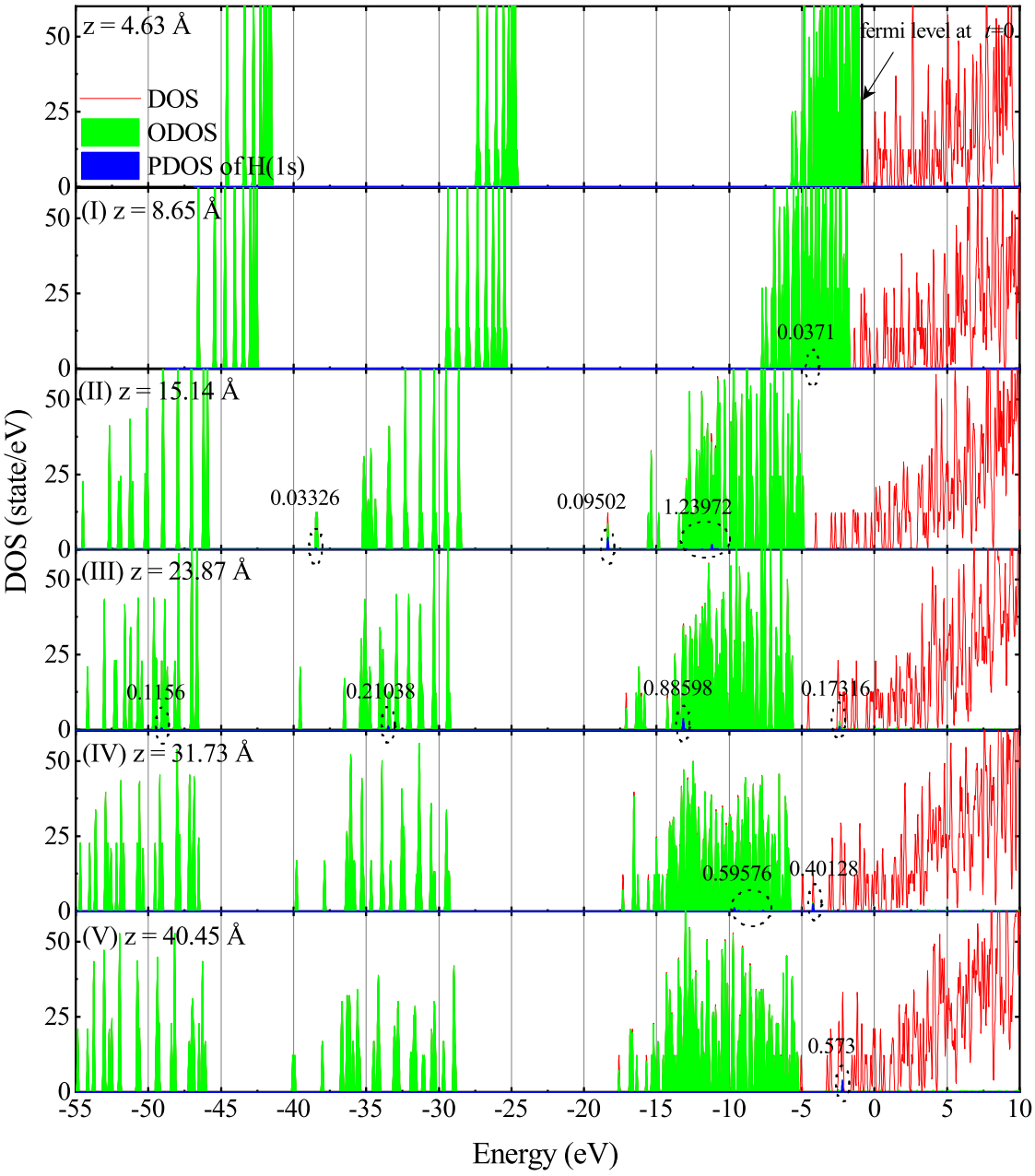

FIG. S6: Snapshots of DOS, ODOS, and PDOS show the projectiles with an incidence velocity of 0.5 a.u. located at z = 4.63, 8.65, 15.14, 23.87, 31.73, and 40.45 Å, respectively, under channel-1. The initial position of the Fermi level is indicated. The dashed ellipse represents the position of the adiabatic eigenstates that contribute to the H(1s) state, while the number of electrons occupying the H(1s) state within the elliptical area is shown above it.

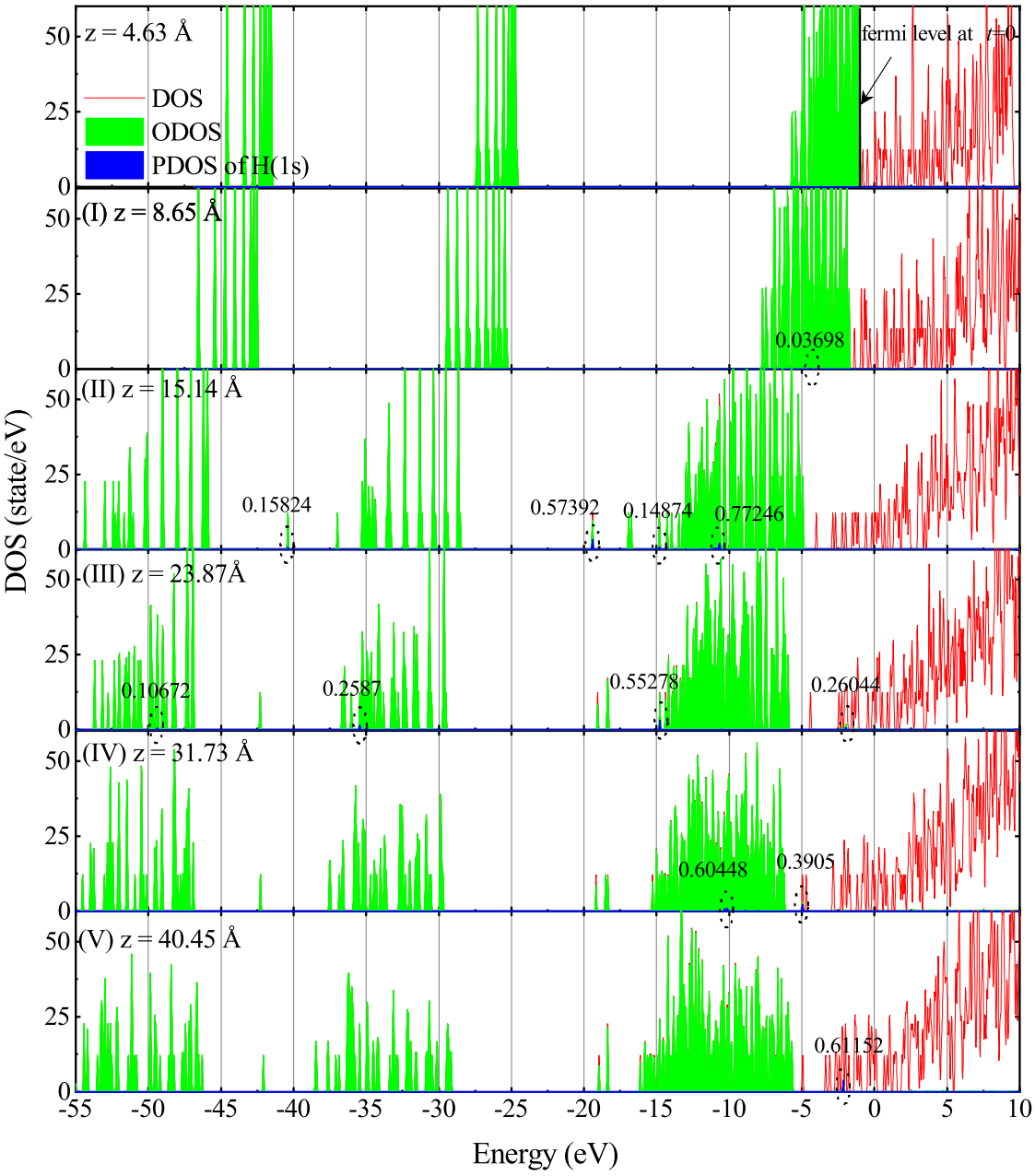

FIG. S7: Same as Figure S6, but under channel-2.

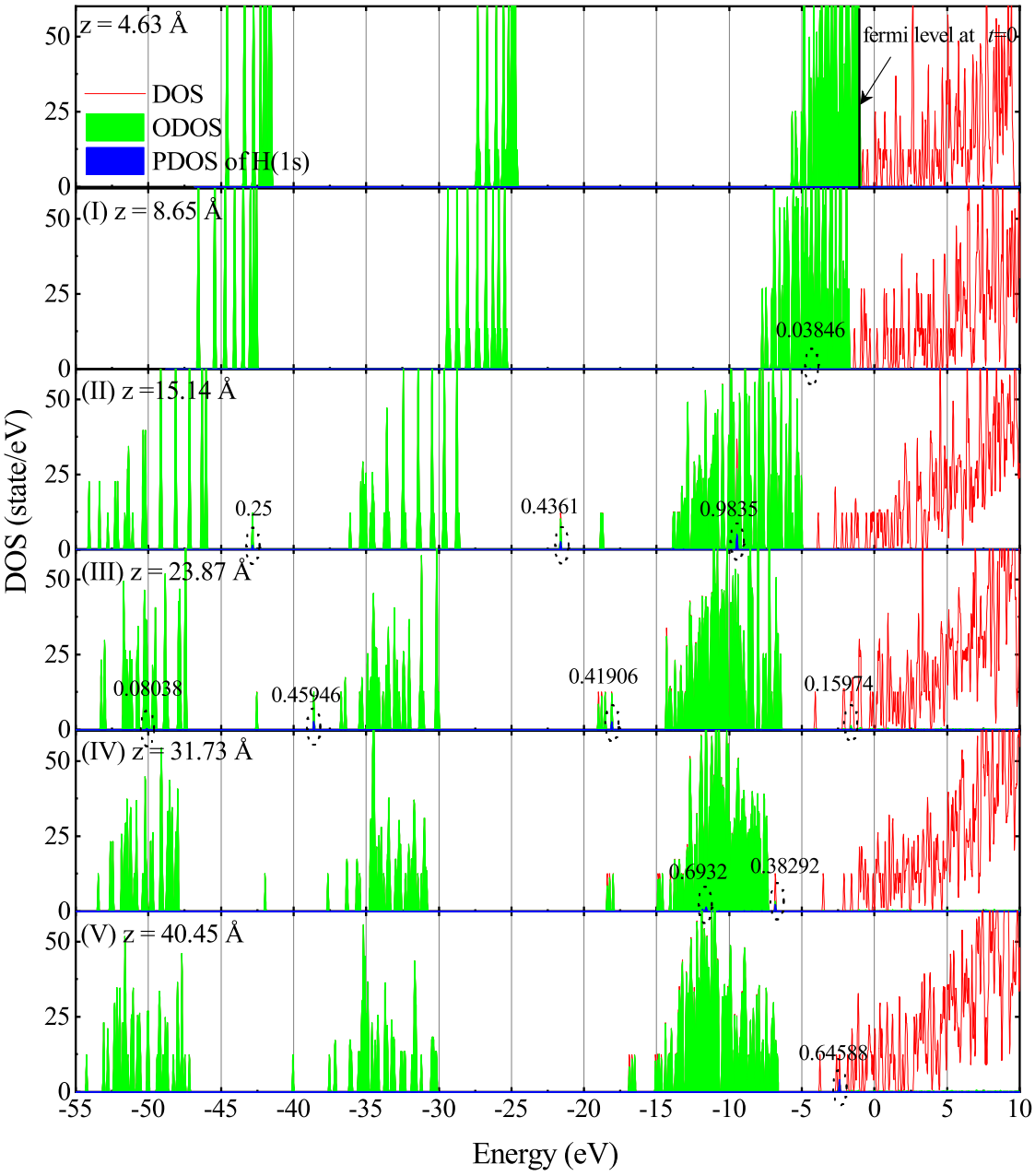

FIG. S8: Same as Figure S6, but under channel-3.

E. Differences in the average electron numbers

In Figure S9, the differences Δn_e in the average electron numbers of F and Li atoms at different energy levels were shown when a proton is incident at a velocity of 0.5 a.u.

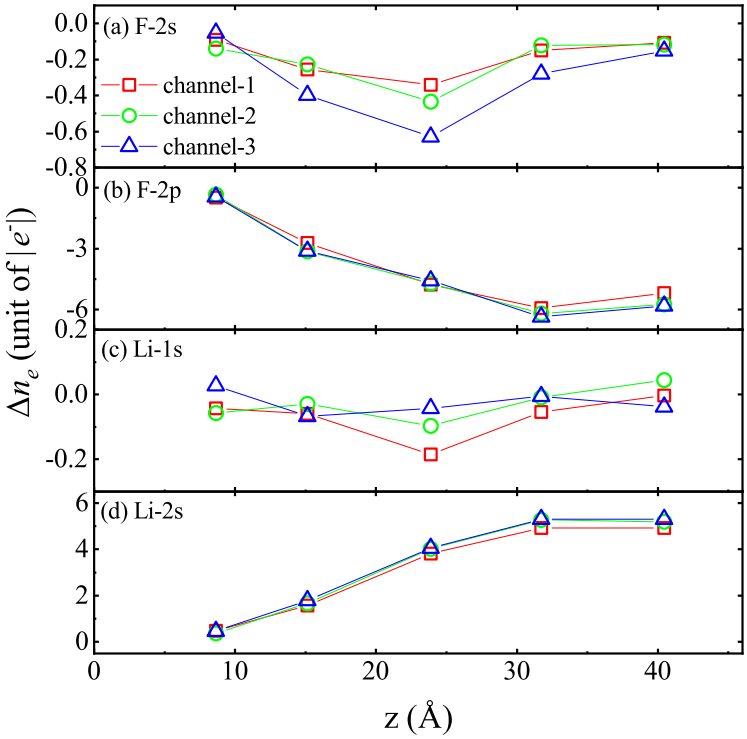

FIG. S9: The differences Δn_e in the average electron numbers of F and Li atoms at different energy levels were shown at z=8.65, 15.14, 23.87, 31.73, and 40.45 Å when a proton is incident at a velocity of 0.5 a.u., where (a) F-2s, (b) F-2p, (c) Li-1s, and (d) Li-2s.